



Present-day shortening in Southern Haiti from GPS measurements and implications for seismic hazard



Steve Symithe^a, Eric Calais^{b,*}

^a Purdue University, Dept. of Earth and Atmospheric Science, West Lafayette, IN, USA

^b Ecole normale supérieure, Dept. of Geosciences, PSL Research University, Paris, France

ARTICLE INFO

Article history:

Received 14 February 2016

Received in revised form 20 April 2016

Accepted 22 April 2016

Available online 29 April 2016

Keywords:

GPS Geodesy

Haiti

Active tectonics

Earthquake hazard

ABSTRACT

The ~3 M inhabitant capital region of Haiti, severely affected by the devastating January 12, 2010, M7.0 earthquake, continues to expand at a fast rate. Accurate characterization of regional earthquake sources is key to inform urban development and construction practices through improved regional seismic hazard estimates. Here we use a recently updated Global Positioning System (GPS) data set to show that seismogenic strain accumulation in southern Haiti involves an overlooked component of shortening on a south-dipping reverse fault along the southern edge of the Cul-de-Sac basin, in addition to the well-known component of left-lateral strike-slip motion. This tectonic model implies that ground shaking may be twice that expected if the major fault was purely strike-slip, as assumed in the current seismic hazard map for the region.

© 2016 Elsevier B.V. All rights reserved.

1. Introduction

On January 12, 2010, Haiti was struck by a devastating – though not unexpected – earthquake (Bilham, 2010) (Fig. 1). Because its epicenter was located in the near vicinity of the Enriquillo Plain Garden Fault (EPGF), a major active fault part of the left-lateral strike-slip boundary between the Caribbean and North American plates (Fig. 1), it was first thought that the event had ruptured a portion of the strike-slip EPGF. Independent studies based on geodetic (Calais et al., 2010; Hayes et al., 2010; Hashimoto et al., 2011; Mercier de Lépinay et al., 2011; Symithe et al., 2013), geological (Prentice et al., 2010), and seismological data (Douilly et al., 2013) showed that the earthquake had actually ruptured a previously unmapped fault with a source mechanism combining strike-slip and reverse faulting, in a setting resembling the 1989 Loma Prieta earthquake in California (e.g., Dietz and Ellsworth, 1990; Beroza, 1991). This composite source mechanism was a first indication that the conventional interpretation of the EPGF in southern Haiti as a purely strike-slip fault system may need revisiting.

GPS measurements in the northeastern Caribbean have established that the 19 mm/yr relative motion between the Caribbean and North American plates, slightly oblique to the plate boundary direction in Hispaniola, is accommodated by shortening on the North Hispaniola fault to the north and strike-slip motion on the ~E–W striking Septentrional and Enriquillo faults throughout the island (Calais et al. (2002), Manaker et al. (2008), Fig. 1). Further geodetic studies making use a

larger number of geodetic sites identified an additional component of boundary–normal shortening in southern Haiti (Calais et al., 2010; Benford et al., 2012; Symithe et al., 2015), consistent with the composite source mechanism of the 2010 earthquake but, again, questioning the purely strike-slip nature of the EPGF system in the region (Mann et al., 1995).

Here, we revisit the present-day tectonic setting of southern Haiti by testing published tectonic models in light of geodetic data acquired since the 2010 earthquake. We show that the well-known strike-slip motion affecting the area is accompanied by an even larger component of shortening on a south-dipping reverse fault along the southern edge of the Cul-de-Sac basin, which holds the ~3 M people capital city of Port-au-Prince. This tectonic scenario implies that ground shaking may be twice that expected if the major fault was purely strike-slip, as assumed in the current seismic hazard map for the region.

2. Tectonic setting

The EPGF has long been recognized as a major tectonic feature of southern Haiti, where it was first named “*Linéament Tiburon-Pétionville*” from the eponymous end-points of its surface trace mapped using airphoto interpretation (Duplan, 1975), then “*Décrochement Sénéstre Sud Haïtien*” (Calmus, 1983). Subsequent studies however tended to minimize its importance as an active plate boundary fault. The EPGF does not appear as a major feature on the 250,000th Haiti geological maps (Moplaisir and Boisson, 1988). Pubellier et al. (1991) proposed that slip on the EPGF stopped in the Late Miocene when deformation in southern Hispaniola became compressional as the Haiti fold-and-thrust belt (Fig. 1) was propagating southward to its present position with its

* Corresponding author at: Ecole normale supérieure, Dept. of Geosciences, 24 rue Lhomond, 75005 Paris, France.

E-mail address: eric.calais@ens.fr (E. Calais).

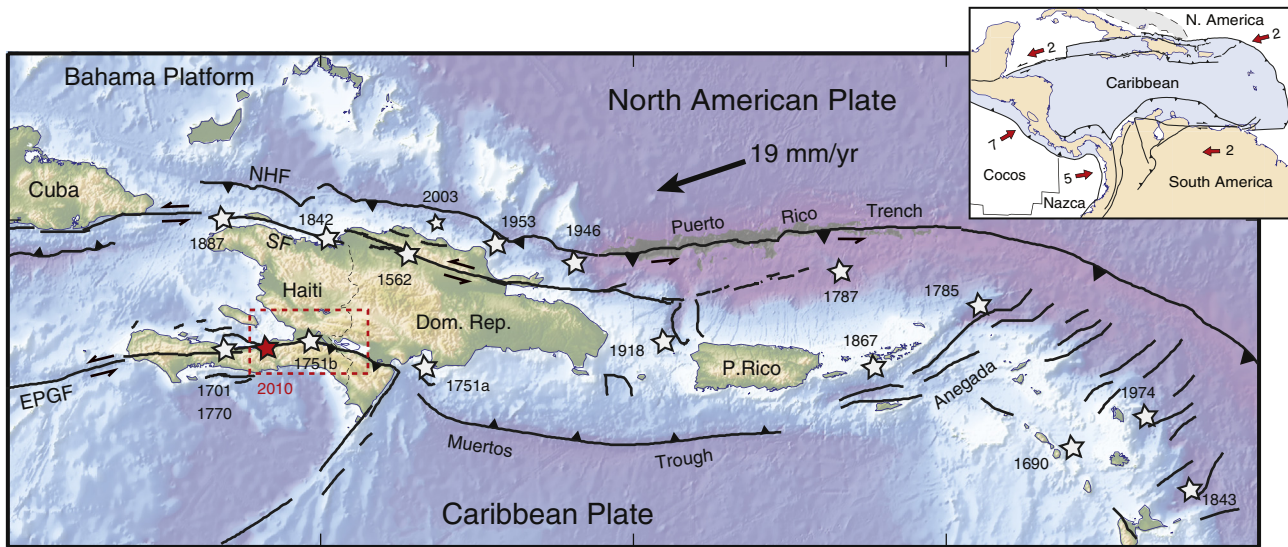


Fig. 1. Current tectonic setting of the northeastern Caribbean. SF = Septentrional fault, EPGF = Enriquillo Plantain Garden Fault. Stars show large ($M < 7$) instrumental and historical earthquakes. Red rectangle shows the area displayed on Fig. 2.

active front currently thrusting onto the Cul-de-Sac basin along the Neiba–Matheux range. In their view, the EPGZ was reactivated as a normal fault in the Quaternary as a result of crustal loading imparted by the fold-and-thrust belt to the north (Pubellier et al., 2000).

Mann et al. (1995) proposed a drastically different interpretation where the EPGF is a quasi-vertical, left-lateral, active strike-slip fault running across southern Hispaniola from the westernmost tip of Haiti to the Enriquillo basin in the Dominican Republic. The fault is indeed well-marked in the morphology throughout the southern Peninsula of Haiti as a quasi-linear feature with push-ups and pull-aparts (Calmus, 1983; Momplaisir, 1986). This holds until about 72.27°W near the city of Pétionville where the EPGF intersects the Cul-de-Sac plain (Fig. 2). East of that point, its imprint on the morphology becomes more subtle. Mann et al. (1995) describe a series of gentle folds affecting plio-quaternary sediments along the southern edge of the Cul-de-Sac basin and into the Enriquillo basin in the Dominican Republic that they interpret as *en échelon* drag folds marking the trace of EPGF (Fig. 2A). The Cabritos island in the Enriquillo lake is the easternmost of these folds and, in that interpretation, is the surface expression of a vertical EPGF at depth. Hence, most of the recent maps show the EPGF as a single – though segmented – left-lateral strike-slip fault extending from Jamaica to the west all the way through southern Haiti and into the Enriquillo basin in the Dominican Republic to the east.

This interpretation contrasts with early geologic work in southern Haiti where the EPGF, well expressed along the Southern Peninsula, is mapped as abutting against a north-verging reverse fault system that mark the southern edge of the Cul-de-Sac basin (Fig. 2B, Bourguieu et al., 1988). Recent geological surveys of the Port-au-Prince area support this interpretation and show that these N110°E reverse-sinistral faults affect Quaternary alluvial sediments throughout the city and to the east (Terrier et al., 2014). At a broader regional scale, Saint Fleur et al. (2015) used high-resolution air photos and lidar topography to revisit the plio-quaternary folds identified by Mann et al. (1995) along the southern edge of the Cul-de-Sac basin. They propose that they are fault-propagation folds on top of shallow-dipping decollements emerging well into the Cul-de-Sac basin and rooted on a south-dipping low-angle reverse fault underneath the high relief Massif de la Selle (Fig. 2B). In their interpretation, the Cul-de-Sac basin is actively overthrust on both sides by the Matheux–Neiba range in the north and the Massif de la Selle in the south while the EPGF is a young (<2 Ma) fault propagating eastward throughout southern Haiti.

3. GPS data

We use GPS data acquired in Haiti and the Dominican Republic since 2003 to test the tectonic models described above, determine the geometry of the major active faults in southern Haiti, and quantify the related elastic strain accumulation to inform regional hazard assessment. GPS data acquisition and processing procedures are provided in Symithe et al. (2013). The solution used here is an improved sub-sample of their data set that includes additional GPS measurements collected in Haiti and the Dominican Republic from June 2014 to April 2015. As a result, we now have a dense distribution of GPS sites covering the whole island, in particular the southern part of Haiti.

The regional velocity field (Fig. 3) shows left-lateral motion between the Caribbean and North American plates at 17–19 mm/yr, slightly oblique to the plate boundary direction. Velocities in Hispaniola show a north–south gradient with up to 15 mm/yr of integrated left-lateral shear strain across the island, consistent with previous findings (Symithe et al., 2015). A new observation, however, is a component of boundary–normal shortening readily visible on Fig. 3. This shortening affects the central and western parts of Hispaniola, except the Southern Peninsula of Haiti west of 72.5°W where velocities in a Caribbean frame are parallel to the E–W-trending EPGF (Calais et al., 2016).

This shortening component, that adds to the well-known regional left-lateral shear, is readily visible on the profile displayed on Fig. 3 where we project the GPS velocities onto directions parallel and normal to the EPGF strike. We observe a well-defined velocity gradient, both in the shortening and strike-slip components, coincident with the contact between the Cul-de-Sac basin and the Massif de la Selle. Although strike-slip motion at about 6–7 mm/yr was expected (Manaker et al., 2008; Benford et al., 2012; Symithe et al., 2015), the significant component of shortening visible on the profiles had not been documented before. In the following, our objective is to determine the geometry of the fault system that accommodates the observed strike-slip and shortening localized along the southern edge of the Cul-de-Sac basin.

4. Elastic model

We implement a simple model where faults are simulated as rectangular dislocations in an elastic half-space. We follow the classically-used backslip approach of Savage (1983) and calculate surface deformation due to faults locked in the upper, seismogenic, crust as the difference

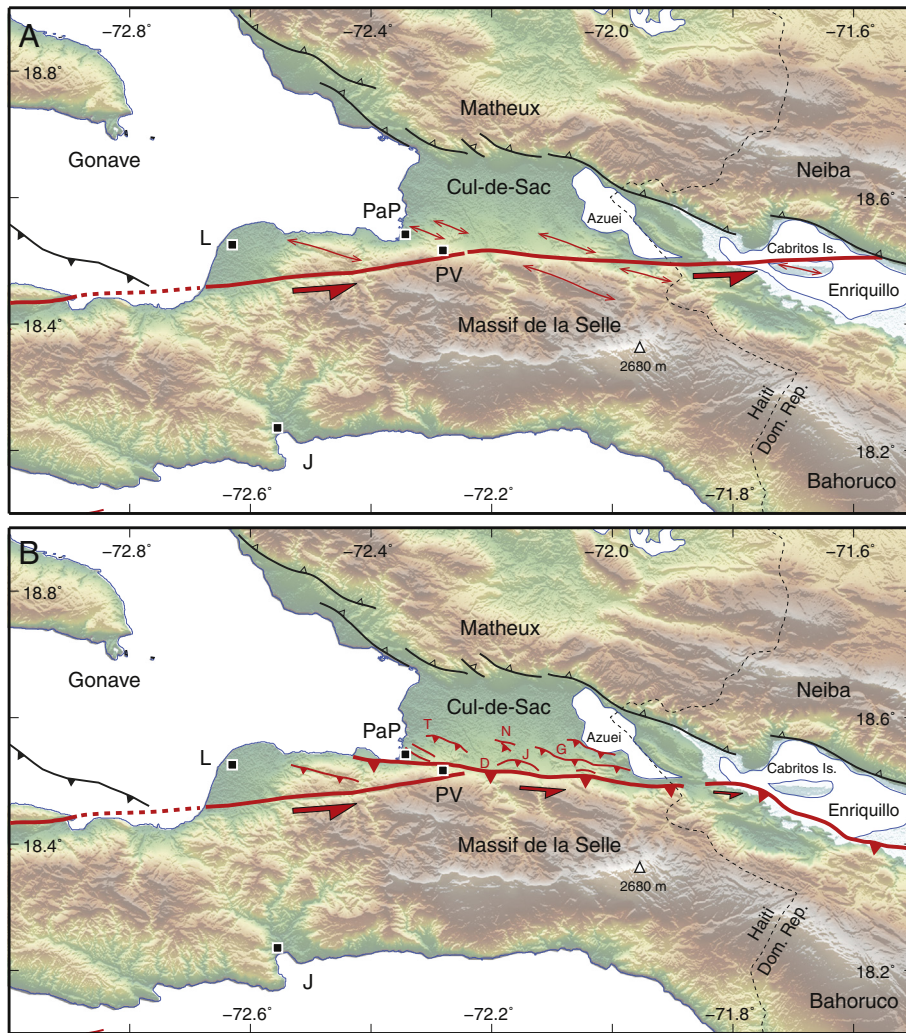


Fig. 2. Comparison of tectonic interpretations of the eastern termination of the Enriquillo fault system. A. Following (Mann et al., 1995), where the Enriquillo fault is a continuous, vertical, strike-slip fault associated with minor en échelon drag folds. B. Following Saint Fleur et al. (2015), where the Enriquillo fault abuts against an oblique-slip fault system with fold-propagation folding well into the Cul-de-Sac basin. T = Tabarre, N = Nan Cadastre, D = Dumay, J = Jacquet, G = Ganthier.

between the deformation caused by an infinitely wide fault plane with uniform slip from the surface downward and the deformation caused by a fault plane with uniform slip across a finite width. We relate fault slip to surface motion using the Green's functions of Okada (1992) for rectangular dislocations assuming uniform slip and dip angle.

In the “one-fault” models, surface deformation is caused by uniform slip on a fault whose dip is varied from 5 to 90, surface trace location from 18.4 to 18.9 latitude, and strike from 70 E to 110 E. In the “two-fault” models, we test whether strike- and dip-slip motion may be partitioned on two different, nearby faults. These fault geometries are obviously simplifications of the actual geology, as GPS measurements are rarely able to capture the details of fault plane geometries, even in regions where dense networks and ample geological data are available (e.g., Argus, 2005). Because the density of GPS sites is not sufficient to capture the short wavelengths of the strain rate field, our models are therefore meant to reproduce the average behavior of a fault system whose geometry is likely to be more complex in actuality.

In order to score the models, we only consider GPS sites that are not affected by fault systems other than the Enriquillo–Cul-de-Sac basin. We model a N–S profile that originates just south of Haiti at longitude 72 W and latitude 17.8 N. We run and score a series of models with profile lengths extending northward from 100 km – i.e., to the southern edge of the Neiba–Matheux mountains – to 200 km – i.e., encompassing additional sites in northern Haiti close to the Septentrional fault (Fig. 5A). As

expected, model misfit increases with profile length as more data is included, but with a significant jump at 180 km profile length, where sites start being significantly affected by elastic strain accumulation on the Septentrional and North Hispaniola faults.

We also run and score a series of models where we vary the profile width to determine reasonable eastern and western bounds for the set of sites to include. We seek to encompass a region where lateral variations in fault geometry and tectonic regime are negligible so that our two-dimensional models hold, while still including as many GPS sites as possible in the analysis. We find that model misfit increases significantly for profile widths of 58 km and larger (Fig. 5B). We therefore select, for the sake of this analysis, GPS sites located inside the 175 km-long by 58 km-wide box shown on Fig. 3.

The model is two-dimensional, though we acknowledge that the study area is not perfectly cylindrical – for instance the EPGF changes direction around 72.27W, as described above. Fig. 5 however shows that all the sites we are using to constrain the models are consistent with a two-dimensional approach. The model used here therefore provides us with a first-order estimate of the active fault geometry at work and allows us to gain new insight into the regional tectonics. A 3-dimensional model will eventually become necessary as our understanding of the local geology allows us to build better-constrained geometries and as the GPS data become more dense, in particular along the southern edge of the Cul-de-Sac basin.

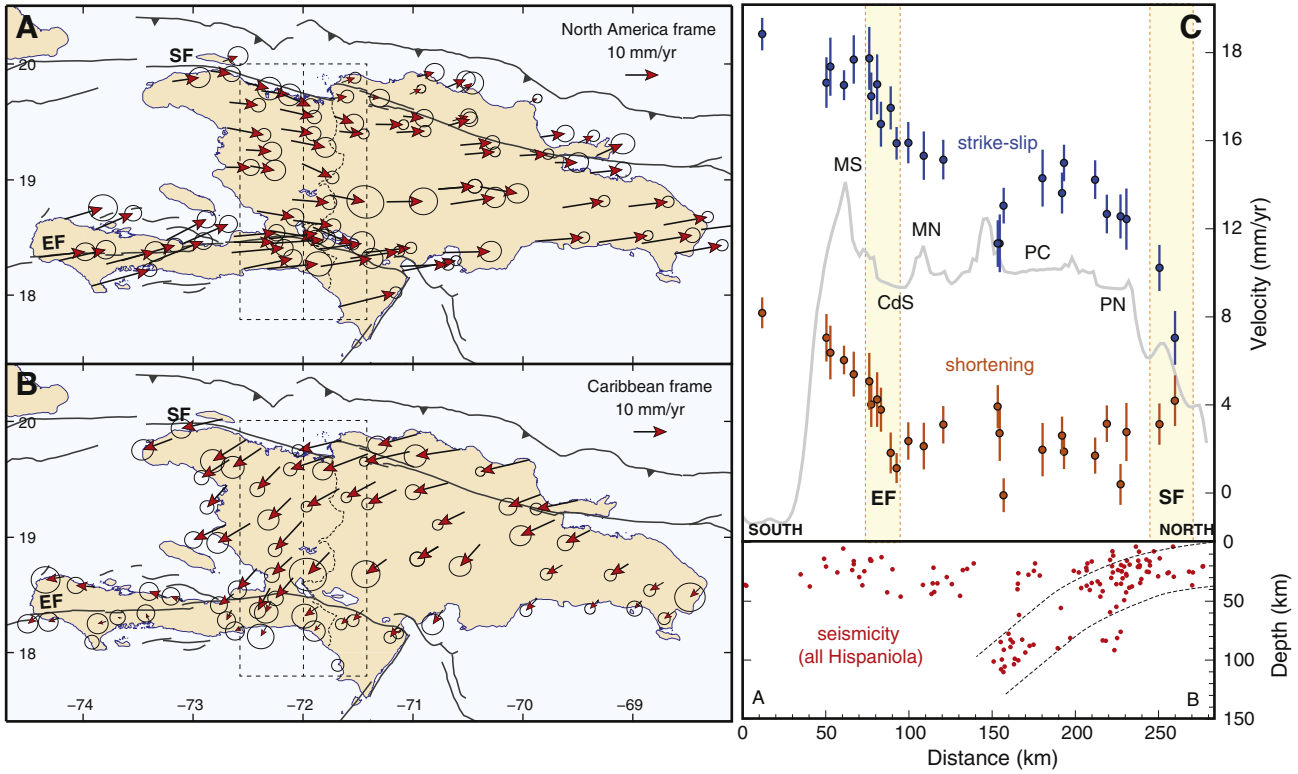


Fig. 3. GPS velocities shown with respect to the North American plate (A) and to the Caribbean plate (B). Error ellipses are 95% confidence. (C) North–south profile including GPS sites shown with the dashed box shown on panels A and B. Velocities are projected onto directions parallel (blue) and normal (red) to the EPGF direction. MS = Massif de la Selle, CdS = Cul-de-Sac basin, MN = Matheux-Neiba range, PC = Plateau Central, PN = Plaine du Nord, EF = Enriquillo fault, SF = Septentrional fault.

In order to optimally search the parameter space and determine reliable uncertainties associated with the estimated parameters, we make use of Bayes' rule (Segall, 2002; Johnson, 2004; Hilley et al., 2005):

$$P(m_i|x) = \frac{P(x|m_i) * P(m_i)}{\sum_j P(x|m_j) * P(m_j)} \quad (1)$$

where m_i is a vector of four unknown parameters (slip, dip, locking depth, and fault location), x is a set of observed GPS velocities, $P(m_i|x)$ is the probability of parameter set m_i to explain the observed data set x , and $P(m_i)$ is some prior probability that this model parameter set actually occurs derived from independent information. $P(x|m_i)$ is the probability of observing x as interseismic surface deformation when the model parameter is m_i . Since we have minimum a priori information on the estimated parameters, we use a uniform distribution as prior for all parameters $P(m_i)$ over intervals 0–20 mm/an for slip rates, 0–90 for dip angle, and 2–15 km for locking depth. In order to optimally evaluate Eq. (1), we use a Metropolis–Hastings sampling method which uses a Markov Chain with stationary distribution (Metropolis et al., 1953).

The best-fit model in the one-fault configuration, shown on Fig. 4, is obtained for a fault–surface intersection at 18.55 latitude, with a dip of 36 ± 13 to the south underneath the Massif de la Selle, and a locking depth of 8 ± 4 km (Table 1). It is remarkable that the inferred location of the fault–surface intersection coincides precisely with the southern toe of the fault-propagating folds identified by Saint Fleur et al. (2015), for instance the Ganthier fold (Fig. 4, bottom panel). The model scores a χ^2 of 69.92 with WRMS of 1.3 mm/yr and 0.8 mm/yr for the E–W and N–S components of the GPS velocities, respectively. Parameters inferred from the Bayesian analysis, their uncertainties, and their covariance are shown on Fig. 6. We observe that inferred parameters are well determined from the data, which favor a south-dipping fault with oblique slip whose tip crops out within the Cul-de-Sac basin.

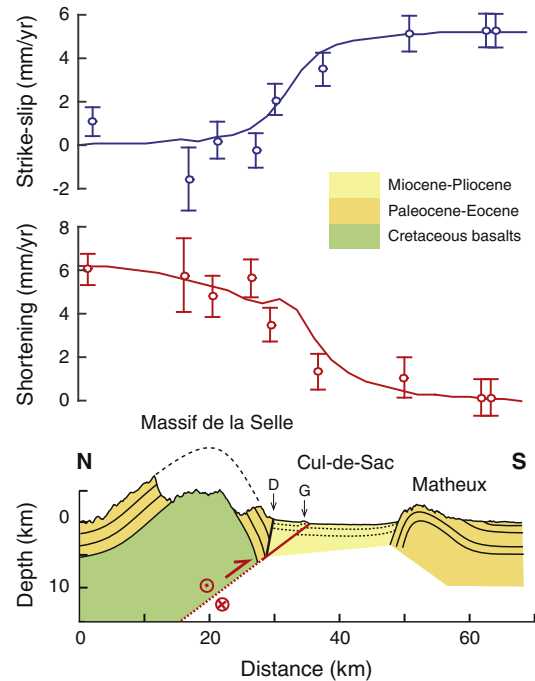


Fig. 4. Top and middle: comparison between the best-fit model (solid lines) and GPS observations for the strike-slip (blue) and shortening (red) components for the one-fault model, i.e. with oblique slip on the south-dipping fault. Bottom: interpretative geological cross-section using information from Saint Fleur et al. (2015). The red line indicates the model fault with its locked portion shown as solid. The surface trace of the fault in the best-fit model coincides with the northern limb of the Ganthier fold, indicated by the letter G. The gradient of GPS velocities coincides with the southern edge of the Cul-de-Sac basin, while the Matheux range appears devoid from present-day strain accumulation. D = Dumay locale where Terrier et al. (2014) report reverse faulting affecting Quaternary sediments. G = Ganthier fold (Mann et al., 1995).

Table 1
Estimated model parameters and associated uncertainties (one-fault model).

Estimated Parameters	Average	Optimum	Std. deviation
Strike-slip rate (mm/yr)	5.7	6.0	2.4
Dip-slip rate (mm/yr)	8.9	9.0	2.8
Dip angle (°)	37.0	36.0	13.0
Locking depth (km)	5.3	6.3	3.5

We also tested a two-fault model where deformation is partitioned onto (1) pure dip-slip motion on the best-fit shallow-dip reverse fault determined above, and (2) pure strike-slip motion on a vertical fault located at the contact between the Massif de la Selle and Cul-de-Sac basin, i.e., the usually assumed EPGF fault geometry. The best-fit slip rates are 6 mm/yr and 9 mm/yr for the strike-slip and reverse faults, similar to the one-fault model. This model scores a χ^2 of 78.62 with WRMS of 1.3 mm/yr and 0.8 mm/yr for the E–W and N–S components of the GPS velocities, respectively. Decreasing the dip of the strike-slip fault systematically increases the misfit (WRMS = 1.35 mm/yr and χ^2 = 85.88 for a 70 dip). Therefore, although partitioning slip on two faults slightly increases the model misfit compared to the one-fault model, the overall fit remains reasonable. However, the data still requires a significant amount of dip-slip motion on a shallow, south-dipping reverse fault with a surface trace located well within the Cul-de-Sac basin.

5. Discussion

5.1. Present-day tectonic model

The modeling of the GPS velocities described above allows us to identify oblique slip on a reverse, south-dipping fault along the southern edge of the Cul-de-Sac basin, with dip-slip exceeding strike-slip velocities. The geodetic data support elastic strain accumulation on a locked, shallow-angle fault dipping southward underneath the Massif de la Selle and accommodating a combination of 9 ± 3 mm/yr of reverse motion and 6 ± 2 mm/yr of strike-slip motion. It is readily apparent on Fig. 4 that the GPS data do not indicate significant deformation along the Neiba–Matheux front at the precision level of the measurements, about 1 mm/yr. We now discuss how this new result fits the geological framework, starting from the broader regional scale.

Plate boundary deformation in southern Hispaniola is currently accommodated by a combination of plate boundary-parallel strike slip motion that appears to decrease from west to east and plate boundary-normal shortening that decreases from west to east (Fig. 3). West of Port-au-Prince, the GPS velocities imply that deformation is partitioned between strike-slip on the EPGF along the Southern Peninsula of Haiti

and shortening across the Gulf of Gonave. This is consistent with seismic surveys that have long shown a series of active folds and reverse faults along the northern coast of the Southern Peninsula and across the Gonave Gulf, the Gonave Island itself being one of these anticlinal folds (Goreau, 1981; Bruneton et al., 1988; Momplaisir, 1986). One of these reverse faults, the Trois Baies fault, was the locus of triggered seismicity with purely reverse focal mechanisms in the wake of the 2010 Haiti earthquake (Douilly et al., 2013).

The reverse faulting required by the GPS data along the southern edge of the Cul-de-Sac basin is consistent with geological observations of active folding (Mann et al., 1995; Terrier et al., 2014) and with the geological interpretation that the Massif de la Selle is actively thrusting over the Cul-de-Sac basin (Bourgueil et al., 1988; Saint Fleur et al., 2015). It remains possible that the strike-slip component is accommodated by an additional, EPGF-type vertical fault, different but close to the reverse fault required by the data. However, the configuration where a strike-slip and a dip-slip fault would intersect at depth does not appear to be mechanically stable – it is difficult to imagine how the two faults would coexist over the long term unless one of them has a very low slip rate, which is not the case with dip-slip and strike-slip components of 9 and 6 mm/yr, respectively.

In addition, the existence of a vertical strike-slip fault along the southern edge of the Cul-de-Sac basin remains elusive, while there is direct field evidence for reverse faulting in Quaternary alluvial deposits throughout Port-au-Prince (Terrier et al., 2014) and just to the east of the city at the Dumay locale (Saint Fleur et al., 2015). These recent observations are consistent with an early geologic map of Haiti where the southern edge of the Cul-de-Sac basin is a north-verging reverse fault system intersecting the EPGF just east of Port-au-Prince (Bourgueil et al., 1988).

The interpretation of a vertical EPGF continuous throughout the Cul-de-Sac basin owes to Mann et al.'s (1995) reproduction of a seismic line across the Enriquillo Lake (MOBIL LINE 1127) in the Dominican Republic where recent faulting just north of the Cabritos Island anticline is interpreted as the trace of the EPGF. However, seismic reflectors below about 1.5 s on this profile are well-marked and continuous across it, indicating that surface faulting does not continue vertically at depth. This points to an alternative interpretation where the Cabritos anticline may be unrelated to the EPGF, but rather be a fault-propagation fold developing above a shallow decollement rooted to the south on a south-dipping reverse fault underneath the Selle-Bahoruco Massif, similar to the interpretation of the Cul-de-Sac folds by Saint Fleur et al. (2015).

We therefore conclude that the geodetic and geological information currently available are consistent with significant present-day shortening coincident with the southern edge of the Cul-de-Sac basin, in addition to

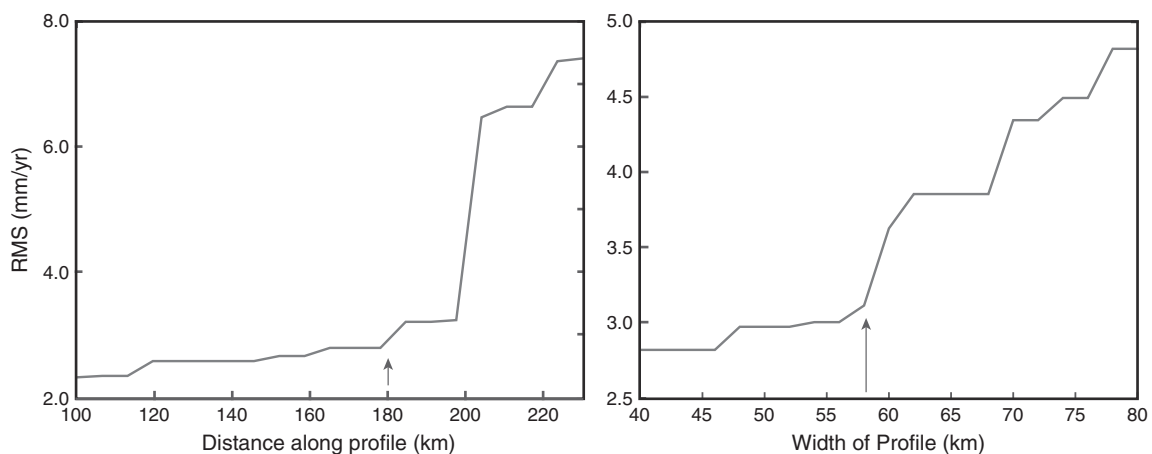


Fig. 5. Model χ^2 as a function of profile length and width. This serves to determine the GPS sites that are not affected by fault systems other than the Enriquillo-Cul-de-Sac basin and for which the two-dimensional fault models used here hold.

the strike-slip motion component also required to fit the geodetic data. We discuss below how this new interpretation of active tectonics in southern Haiti affects hazard estimates in the Port-au-Prince region.

5.2. Implication for seismic hazard

The current Haiti seismic hazard maps, produced shortly after the 2010 earthquake (Frankel et al., 2011), follow the Mann et al. (1995) interpretation of a vertical, purely strike-slip EPGF throughout southern Haiti and include active reverse faulting along the Matheux-Neiba front. The tectonic scenario advocated here on the basis of GPS data is different. We therefore seek to determine the impact of either scenario on seismic ground motion. To do so, we follow the ShakeMap procedure (Wald et al., 1999) using the openSHA framework (Field et al., 2005).

In the alternate tectonic scenario advocated in this paper, we assume a finite source rupture on a fault dipping 36° to the south, parallel to the reverse faults mapped by Saint Fleur et al. (2015) along the southern edge of the Cul-de-Sac basin (Fig. 2B). We simulate a rupture of magnitude 7.0, consistent with historical records in the region (Ali et al., 2008; Bakun et al., 2012). We model a rupture plane extending laterally from 72.35 W/18.56 N to 71.88 W/18.506 N (i.e., 50 km-long) and vertically from 0 to 6 km (i.e., 10 km rupture width for a 36° dip), combining dip-slip and strike-slip motion with a rake of 56°. In the classic EPGF scenario, we assume a finite source rupture on a vertical fault following the trace shown in Mann et al. (1995) and used in (Frankel et al., 2011) (Fig. 2A). We use the same lateral extent as in the alternate scenario with a vertical extent from 0 to 10 km and pure strike-slip motion (rake = 0°).

All other simulation parameters are identical for both scenarios. We use the same attenuation relations as in the 2010 Haiti national seismic hazard maps (Frankel et al., 2011) which apply with equal weight three of the Next Generation of Attenuation (NGA) relations (Boore and Atkinson, 2008; Campbell and Bozorgnia, 2008; Chiou and Youngs, 2008), derived from a global compilation of strong-motion records from tectonically active areas. The additional details provided by the microzonation study of Port-au-Prince (Gilles et al., 2013) are unimportant for our discussion. We make use of Vs30 estimations from topographic slope derived from SRTM30 Version 2 (Allen and Wald, 2009). Fig. 7 shows the resulting maps of the median peak ground acceleration (PGA) for the two scenarios described above. They are meant to qualitatively illustrate these scenarios – exploring other attenuation relations or producing an actual seismic hazard map is beyond the scope of this paper.

We observe contrasted results between the two scenarios, with PGA reaching 0.5 g for the vertical strike-slip rupture but up to 0.80 g for the oblique-slip rupture on a south-dipping fault ($g = 9.82 \text{ m s}^{-2}$). The

new interpretation of the Cul-de-Sac basin tectonic regime required by the geodetic data is therefore much more detrimental for southern Haiti than the strike-slip source assumed in the current earthquake hazard maps. This holds in particular for the Port-au-Prince area where ground acceleration was likely limited to 0.1–0.4 g during the 2010 earthquake according to models (Mavroeidis and Scotti, 2013; Douilly et al., 2015) and geotechnical analysis of ground performance (Olson et al., 2011).

6. Conclusion

An improved GPS data set across Haiti shows that active strain accumulation in the southern part of the island involves a significant component of north–south shortening in addition to the well-known component of left-lateral strike-slip motion. Horizontal gradients in GPS velocities together with simple elastic models require that this deformation is accommodated by a combination of reverse ($9 \pm 3 \text{ mm/yr}$) and strike-slip ($6 \pm 2 \text{ mm/yr}$) faulting on active faults along the southern edge of the Cul-de-Sac basin. The data is consistent with oblique motion accommodated by a fault dipping at a shallow angle of $36^\circ \pm 13^\circ$ under the Massif de la Selle with the surface trace located well within the Cul-de-Sac basin, in agreement with the location of fault-propagation folds described in the basin morphology (Saint Fleur et al., 2015).

This new interpretation has important implications for seismic hazard as rupture on the reverse or oblique fault required by the geodetic data implies ground motion that may be up to twice larger than rupture on the usually assumed vertical, purely strike-slip, EPGF. There is much at stake in this ~3 M inhabitant region that is still recovering from the 2010 earthquake and where urbanization continues at a fast rate. Additional geodetic and geological work in this region is key to further investigate this interpretation and, eventually, lead to revised and improved seismic hazard estimates for the region.

The rupture area modeled above is consistent with a Mw7.0 event according to commonly used earthquake scaling laws (Stirling et al., 2013). For a shear modulus of 33 GPa, the simulated earthquake amounts to a uniform coseismic slip of 2.5 m. At the loading rate derived here from the GPS data, this implies a 223 year repeat time if the system is at steady-state and such earthquakes are characteristic. Given the lack of large earthquakes on the Cul-de-Sac segment of the Enriquillo fault system since the series of large and devastating events of the eighteenth century (Fig. 1), it is clear that the capital region of Haiti must prepare for future earthquakes that could unfortunately cause significantly stronger ground motion – and damage – than experienced during the 2010 event.

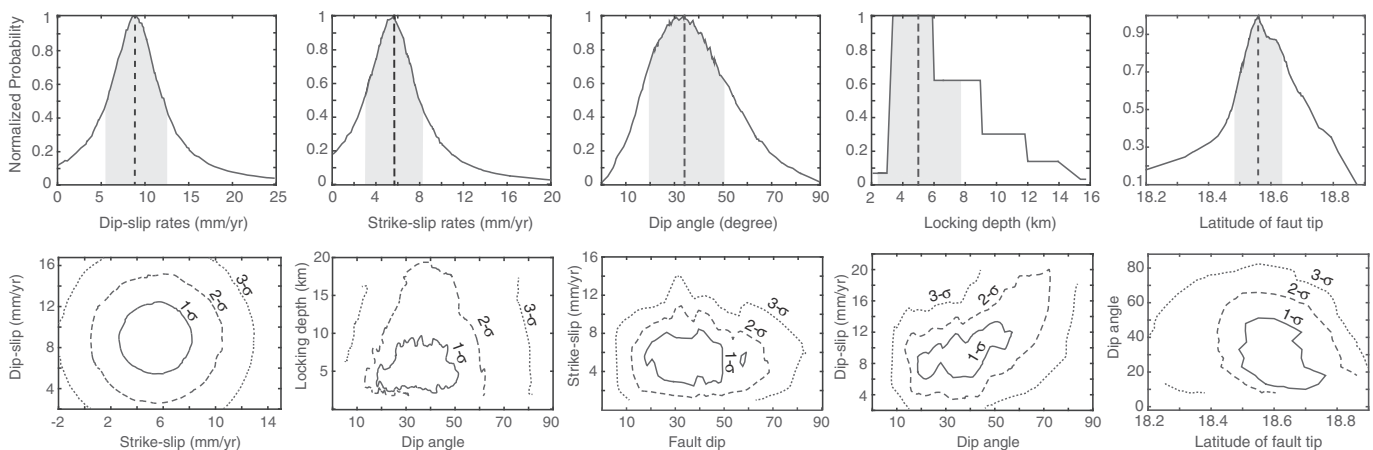


Fig. 6. Top row: parameter estimates for strike-slip rate, dip-slip rate, locking depth, and locking depth. Gray area shows the standard deviation. Bottom row: covariations of parameter estimates. The latitude of the fault tip is the fault–surface intersection.

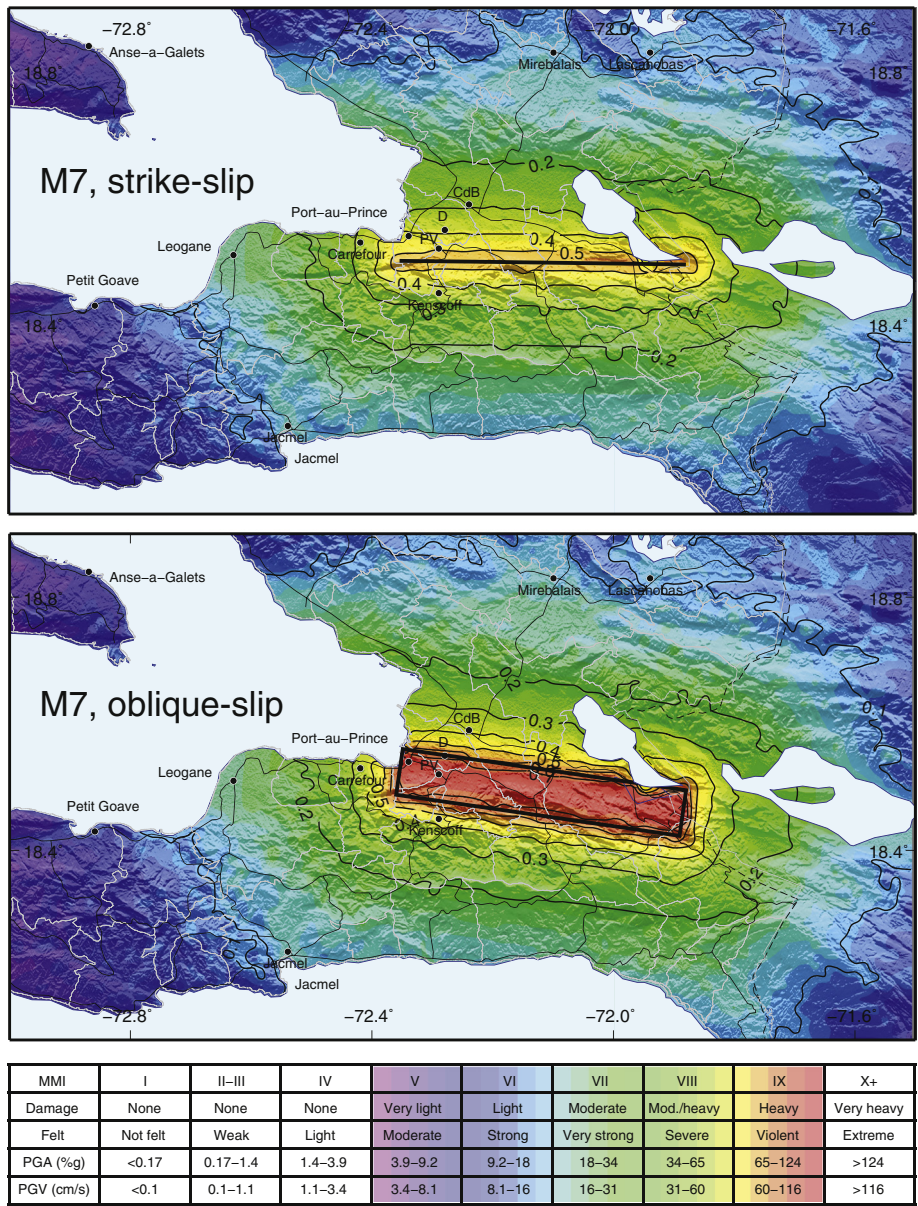


Fig. 7. Ground motion scenarios illustrating the two end-member models discussed in the text. Thick black lines show the surface projection of the simulated rupture, of magnitude 7.0 in both cases. Solid contours show PGA in g. Background colors show modified Mercalli intensities calculated according to Wald et al. (1999). CdB = Croix des Bouquets, D = Delmas, PV = Pétionville.

Acknowledgments

The campaign GPS data used in this study were collected as part of the “CANAPE” (Caribbean North America Plate Experiment) project with support from the Dirección General de Minería, the Instituto Cartográfico Militar, the Colegio Dominicano de Ingenieros, Arquitectos y Agrimensores (CoDIA), and Holasa S.A. in the Dominican Republic and from the Bureau des Mines et de l’Energie, the Direction de la Protection Civile, the Centre National de l’Information Géospatiale, and the Faculté des Sciences de l’Université d’Etat in Haiti. We used all publicly available continuous data from various providers, in particular the “COCONet” (Continuously Operating Caribbean Observation Network, coconet.unavco.org) international initiative and the U.S. “CORS” network (Continuously Operating Reference Stations geodesy.noaa.gov/CORS/). We thank N. Saint Fleur, N. Feuillet, and Y. Klinger for sharing geological information and interpretation ahead of publication. We thank K. Vanneste and T. Camelbeek for taking the time to double-check our ground motion calculations. This work benefited from insightful discussions with B. de

Lépinay. We thank reviewers P. Vernant and R. Bilham, as well as editor R. Govers for their constructive comments. This research was supported by a COCONet fellowship from UNAVCO (EAR-1042906/EAR-1042909) to SJS and National Science Foundation awards EAR-0409487, EAR-RAPID-1024990, and EAR-1045809 to EC.

References

Ali, S.T., Freed, A.M., Calais, E., Manaker, D.M., McCann, W.R., 2008. Coulomb stress evolution in Northeastern Caribbean over the past 250 years due to coseismic, postseismic and interseismic deformation. *Geophys. J. Int.* 174 (3), 904–918.
 Allen, T.I., Wald, D.J., 2009. On the use of high-resolution topographic data as a proxy for seismic site conditions (VS30). *Bull. Seismol. Soc. Am.* 99 (2A), 935–943.
 Argus, D.F., 2005. Interseismic strain accumulation and anthropogenic motion in metropolitan Los Angeles. *J. Geophys. Res.* 110, B04401.
 Bakun, W.H., Flores, C.H., U. S. ten Brink, 2012. Significant earthquakes on the Enriquillo Fault System, Hispaniola, 1500–2010: implications for seismic hazard. *Bull. Seismol. Soc. Am.* 102 (1), 18–30.
 Benford, B., DeMets, C., Calais, E., 2012. GPS estimates of microplate motions, northern Caribbean: evidence for a Hispaniola microplate and implications for earthquake hazard. *Geophys. J. Int.* 191 (2), 481–490.

- Beroza, G.C., 1991. Near-source modeling of the Loma Prieta earthquake: evidence for heterogeneous slip and implications for earthquake hazard. *Bull. Seismol. Soc. Am.* 81 (5), 1603–1621.
- Bilham, R., 2010. Structural geology: invisible faults under shaky ground. *Nat. Geosci.* 3 (11), 743–745.
- Boore, D.M., Atkinson, G.M., 2008. Ground-motion prediction equations for the average horizontal component of PGA, PGV, and 5 sand 10.0 s. *Earthquake Spectra* 24 (1), 99–138.
- Bourguéil, B., Andreieff, P., Lasnier, J., Gonnard, R., Le Metour, J., Rancon, J.-P., 1988. Synthèse Géologique de la République d'Haiti. Technical report, Bureau des Mines et de l'Energie. Haiti, Port-au-Prince.
- Bruneton, A., Gonnard, R., Gou, Y., Lasnier, J., Negroni, P., 1988. Evaluation du potentiel pétrolier, Synthèse géologique de la République d'Haiti. Technical Report BME/BID ATN-SA 2506-HA, Bureau des Mines et de l'Energie. Haiti, Port-au-Prince.
- Calais, E., Freed, A., Mattioli, G., Amelung, F., Jonsson, S., Jansma, P., Hong, S.-H., Dixon, T., Prépétit, C., Mompalaisir, R., 2010. Transpressional rupture of an unmapped fault during the 2010 Haiti earthquake. *Nat. Geosci.* 3 (11), 1–6.
- Calais, E., Mazabraud, Y., de Lépinay, B.M., Mann, P., Mattioli, G.S., Jansma, P., 2002. Strain partitioning and fault slip rates in the northeastern Caribbean from GPS measurements. *Geophys. Res. Lett.* 29 (18), 1856.
- Calais, E., Symithe, S., de Lépinay, B., Prépétit, C., 2016. Plate boundary segmentation in the northeastern Caribbean from geodetic measurements and Neogene geological observations. *Compt. Rendus Geosci.* 348 (1), 42–51.
- Calmus, T., 1983. Contribution à l'étude géologique du massif de Macaya (sud-ouest d'Haiti, Grandes Antilles), sa place dans l'orogène nord caraïbe (Ph. D. thesis, Paris, France).
- Campbell, K.W., Bozorgnia, Y., 2008. NGA ground motion model for the geometric mean horizontal component of PGA, PGV, PGD and 5 ranging from 0.01 to 10 s. *Earthquake Spectra* 24 (1), 139–171.
- Chiou, B.-J., Youngs, R.R., 2008. An NGA model for the average horizontal component of peak ground motion and response spectra. *Earthquake Spectra* 24 (1), 173–215.
- Dietz, L.D., Ellsworth, W.L., 1990. The October 17, 1989, Loma Prieta, California, earthquake and its aftershocks: geometry of the sequence from high-resolution locations. *Geophys. Res. Lett.* 17 (9), 1417–1420.
- Douilly, R., Aochi, H., Calais, E., Freed, A.M., 2015. Three-dimensional dynamic rupture simulations across interacting faults: the Mw7.0, 2010, Haiti earthquake. *J. Geophys. Res. Solid Earth* 120 (2), 1108–1128.
- Douilly, R., Haase, J.S., Ellsworth, W.L., Bouin, M.P., Calais, E., Symithe, S.J., Armbruster, J.G., de Lépinay, B.M., Deschamps, A., Mildor, S.L., Meremonte, M.E., Hough, S.E., 2013. Crustal structure and Fault geometry of the 2010 Haiti earthquake from temporary seismometer deployments. *ol. Soc. Am.* 103 (4), 2305–2325.
- Duplan, L., 1975. Carte Structurale de la République d'Haiti. Région Sud.
- Field, E.H., Seligson, H.A., Gupta, N., Gupta, V., Jordan, T.H., Campbell, K.W., 2005. Loss estimates for a Puente Hills blind-thrust earthquake in Los Angeles, California. *Earthquake Spectra* 21 (2), 329–338.
- Frankel, A., Harmsen, S., Mueller, C., Calais, E., Haase, J., 2011. Seismic hazard maps for Haiti. *Earthquake Spectra* 27 (S1), S23–S41.
- Gilles, R., Bertil, D., Prépétit, C., Belvaux, M., Roullé, A., Jean-Philippe, J., Noury, G., 2013. Seismic microzoning in the metropolitan area of Port-au-Prince: complexity of the subsoil. *American Geophysical Union Fall Meeting*, San Francisco, pp. Abstract S51A-2312.
- Goreau, P., 1981. The Tectonic Evolution of the North Central Caribbean Plate Margin (Master's thesis, MIT).
- Hashimoto, M., Fukushima, Y., Fukahata, Y., 2011. Fan-delta uplift and mountain subsidence during the Haiti 2010 earthquake. *Nat. Geosci.* 4 (4), 1–5.
- Hayes, G.P., Briggs, R.W., Sladen, A., Fielding, E.J., Prentice, C., Hudnut, K., Mann, P., Taylor, F.W., Crone, A.J., Gold, R., Ito, T., Simons, M., 2010. Complex rupture during the 12 January 2010 Haiti earthquake. *Nat. Geosci.* 3 (11), 800–805.
- Hilley, G.E., Bürgmann, R., Zhang, P.Z., 2005. Bayesian inference of plastosphere viscosities near the Kunlun Fault, northern Tibet. *Geophys. Res. Lett.* 32, L01302.
- Johnson, K.M., 2004. Viscoelastic earthquake cycle models with deep stress-driven creep along the San Andreas fault system. *J. Geophys. Res.* 109, B10403.
- Manaker, D.M., Calais, E., Freed, A.M., Ali, S.T., Przybylski, P., Mattioli, G., Jansma, P., Prépétit, C., de Chabaliér, J.B., 2008. Interseismic plate coupling and strain partitioning in the Northeastern Caribbean. *Geophys. J. Int.* 174 (3), 889–903.
- Mann, P., Taylor, F.W., Edwards, R.L., Ku, T.L., 1995. Actively evolving microplate formation by oblique collision and sideways motion along strike-slip faults: an example from the northeastern Caribbean plate margin. *Tectonophysics* 246 (1–3), 1–69.
- Mavroeidis, G.P., Scotti, C.M., 2013. Finite-fault simulation of broadband strong ground motion from the 2010 Mw 7.0 Haiti earthquake. *Bull. Seismol. Soc. Am.* 103 (5), 2557–2576.
- Mercier de Lépinay, B., Deschamps, A., Klingelhoefer, F., Mazabraud, Y., Delouis, B., Clouard, V., Hello, Y., Crozon, J., Marcaillou, B., Graindorge, D., Vallée, M., Perrot, J., Bouin, M.-P., Saurel, J.-M., Charvis, P., St-Louis, M., 2011. The 2010 Haiti earthquake: a complex fault pattern constrained by seismologic and tectonic observations. *Geophys. Res. Lett.* 38, L22305.
- Metropolis, N., Rosenbluth, A.W., Rosenbluth, M.N., Teller, A.H., Teller, E., 1953. Equation of state calculations by fast computing machines. *J. Chem. Phys.* 21 (6), 1087.
- Mompalaisir, R., 1986. Contribution à l'étude géologique de la partie orientale du massif de la Hotte (Presqu'île du Sud d'Haiti): synthèse structurale des marges de la Presqu'île (Ph. D. thesis, Paris).
- Mompalaisir, R., Boisson, D., 1988. Carte Géologique de la République d'Haiti, South-East sheet (Port-au-Prince) (BME.).
- Okada, Y., 1992. Internal deformation due to shear and tensile faults in a half-space. *Bull. Seismol. Soc. Am.* 82 (2), 1018–1040.
- Olson, S.M., Green, R.A., Lasley, S., Martin, N., Cox, B.R., Rathje, E., Bachhuber, J., French, J., 2011. Documenting liquefaction and lateral spreading triggered by the 12 January 2010 Haiti earthquake. *Earthquake Spectra* 27 (S1), S93–S116.
- Prentice, C.S., Mann, P., Crone, A.J., Gold, R.D., Hudnut, K.W., Briggs, R.W., Koehler, R.D., Jean, P., 2010. Seismic hazard of the Enriquillo–Plantain Garden fault in Haiti inferred from palaeoseismology. *Nat. Geosci.* 3 (11), 1–5.
- Pubellier, M., Mauffret, A., Leroy, S., Vila, J.M., Amilcar, H., 2000. Plate boundary readjustment in oblique convergence: example of the Neogene of Hispaniola, Greater Antilles. *Tectonics* 19 (4), 630–648.
- Pubellier, M., Vila, J.M., Boisson, D., 1991. North Caribbean neotectonic events: the Trans-Haitian fault system. Tertiary record of an oblique transcurrent shear zone uplifted in Hispaniola. *Tectonophysics* 194 (3), 217–236.
- Saint Fleur, N., Feuillet, N., Grandin, R., 2015. Seismotectonics of southern Haiti: a new faulting model for the 12 January 2010 M7 earthquake. *Geophys. Res. Lett.* 42.
- Savage, J.C., 1983. A dislocation model of strain accumulation and release at a subduction zone. *J. Geophys. Res.* 88 (B6), 4984–4996.
- Segall, P., 2002. Integrating geologic and geodetic estimates of slip rate on the San Andreas fault system. *Int. Geol. Rev.* 44 (1), 62–82.
- Stirling, M., Goded, T., Berryman, K., Litchfield, N., 2013. Selection of earthquake scaling relationships for seismic-hazard analysis. *Bull. Seismol. Soc. Am.* 103 (6), 2993–3011.
- Symithe, S., Calais, E., Chabaliér, J.B., 2015. Current block motions and strain accumulation on active faults in the Caribbean. *J. Geophys. Res. Solid Earth* 120 (5), 3748–3774.
- Symithe, S.J., Calais, E., Haase, J.S., Freed, A.M., Douilly, R., 2013. Coseismic slip distribution of the 2010 M 7.0 Haiti earthquake and resulting stress changes on regional faults. *Bull. Seismol. Soc. Am.* 103 (4), 2326–2343.
- Terrier, M., Bialkowski, A., Nachbaur, A., Prépétit, C., Joseph, Y.F., 2014. Revision of the geological context of the Port-au-Prince metropolitan area, Haiti: implications for slope failures and seismic hazard assessment. *Nat. Hazards Earth Syst. Sci.* 14 (9), 2577–2587.
- Wald, D.J., Quitoriano, V., Heaton, T.H., Kanamori, H., 1999. Relationships between peak ground acceleration, peak ground velocity, and modified Mercalli intensity in California. *Earthquake Spectra* 15 (3), 557–564.